UvA-DARE (Digital Academic Repository)

Dijet angular distributions in direct and resolved photoproduction at HERA

Derrick(et al.), M.; Botje, M.A.J.; Chlebana, F.S.; Engelen, J.J.; de Kamps, M.; Kooijman, P.M.; Kruse, A.; van Sighem, A.I.; Tiecke, H.G.J.M.; Verkerke, W.; Vossebeld, J.H.; Vreeswijk, M.; Wiggers, L.W.; de Wolf, E.; van Woudenberg, R.

Link to publication

Dijet angular distributions in direct and resolved photoproduction at HERA

ZEUS Collaboration

M. Derrick, D. Krakauer, S. Magill, D. Mikunas, B. Musgrave, J.R. Okrasinski, J. Repond, R. Stanek, R.L. Talaga, H. Zhang

Argonne National Laboratory, Argonne, IL, USA[51]

M.C.K. Mattingly

Andrews University, Berrien Springs, MI, USA

G. Bari, M. Basile, L. Bellagamba, D. Boscherini, A. Bruni, G. Bruni, P. Bruni, G. Cara Romeo, G. Castellini[1], L. Cifarelli[2], F. Cindolo, A. Contin, M. Corradi, I. Gialas, P. Giusti, G. Iacobucci, G. Laurenti, G. Levi, A. Margotti, T. Massam, R. Nania, F. Palmonari, A. Polini, G. Sartorelli, Y. Zamora Garcia[3], A. Zichichi

University and INFN Bologna, Bologna, Italy[41]

C. Amelung, A. Bornheim, J. Crittenden, R. Deffner, T. Doeker[4], M. Eckert, L. Feld, A. Frey[5], M. Geerts, M. Grothe, H. Hartmann, K. Heinloth, L. Heinz, E. Hilger, H.-P. Jakob, U.F. Katz, S. Mengel[6], E. Paul, M. Pfeiffer, Ch. Rembser, D. Schramm[7], J. Stamm, R. Wedemeyer

Physikalisches Institut der Universität Bonn, Bonn, Germany[38]

S. Campbell-Robson, A. Cassidy, W.N. Cottingham, N. Dyce, B. Foster, S. George, M.E. Hayes, G.P. Heath, H.F. Heath, D. Piccioni, D.G. Roff, R.J. Tapper, R. Yoshida

H.H. Wills Physics Laboratory University of Bristol, Bristol, UK[50]

M. Arneodo[8], R. Ayad, M. Capua, A. Garfagnini, L. Iannotti, M. Schioppa, G. Susinno

Calabria University, Physics Dept. and INFN, Cosenza, Italy[41]

A. Caldwell[9], N. Cartiglia, Z. Jing, W. Liu, J.A. Parsons, S. Ritz[10], F. Sciulli, P.B. Straub, L. Wai[11], S. Yang[12], Q. Zhu

Columbia University, Nevis Labs., Irvington on Hudson, N.Y., USA[52]

P. Borzemski, J. Chwastowski, A. Eskreys, Z. Jakubowski, M.B. Przybycień, M. Zachara, L. Zawiejski

Inst. of Nuclear Physics, Cracow, Poland[45]

L. Adamczyk, B. Bednarek, K. Jeleń, D. Kisielewska, T. Kowalski, M. Przybycień,
E. Rulikowska-Zarębska, L. Suszycki, J. Zając

Faculty of Physics and Nuclear Techniques, Academy of Mining and Metallurgy, Cracow, Poland[45]

Z. Duliński, A. Kotański

Jagellonian Univ., Dept. of Physics, Cracow, Poland[46]

G. Abbiendi[13], L.A.T. Bauerdick, U. Behrens, H. Beier, J.K. Bienlein, G. Cases, O. Deppe,
K. Desler, G. Drews, M. Flasiński[14], D.J. Gilkinson, C. Glasman, P. Göttlicher,
J. Große-Knetter, T. Haas, W. Hain, D. Hasell, H. Heßling, Y. Iga, K.F. Johnson[15], P. Joos,
M. Kasemann, R. Klanner, W. Koch, U. Kötz, H. Kowalski, J. Labs, A. Ladage, B. Löhr,
M. Löwe, D. Lüke, J. Mainusch[16], O. Mańczak, J. Milewski, T. Monteiro[17], J.S.T. Ng,
D. Notz, K. Ohrenberg, K. Piotrzkowski, M. Roco, M. Rohde, J. Roldán, U. Schneekloth,
W. Schulz, F. Selonke, B. Surrow, T. Voß, D. Westphal, G. Wolf, U. Wollmer,
C. Youngman, W. Zeuner

Deutsches Elektronen-Synchrotron DESY, Hamburg, Germany

H.J. Grabosch, A. Kharchilava[18], S.M. Mari[19], A. Meyer, S. Schlenstedt, N. Wulff

DESY-IfH Zeuthen, Zeuthen, Germany

G. Barbagli, E. Gallo, P. Pelfer

University and INFN, Florence, Italy[41]

G. Maccarrone, S. De Pasquale, L. Votano

INFN, Laboratori Nazionali di Frascati, Frascati, Italy[41]

A. Bamberger, S. Eisenhardt, T. Trefzger[20], S. Wölfle

Fakultät für Physik der Universität Freiburg i.Br., Freiburg i.Br., Germany[38]

J.T. Bromley, N.H. Brook, P.J. Bussey, A.T. Doyle, D.H. Saxon, L.E. Sinclair, M.L. Utley,
A.S. Wilson

Dept. of Physics and Astronomy, University of Glasgow, Glasgow, UK[50]

A. Dannemann, U. Holm, D. Horstmann, R. Sinkus, K. Wick

Hamburg University, I. Institute of Exp. Physics, Hamburg, Germany[38]

B.D. Burow[21], L. Hagge[16], E. Lohrmann, G. Poelz, W. Schott, F. Zetsche

Hamburg University, II. Institute of Exp. Physics, Hamburg, Germany[38]

T.C. Bacon, N. Brümmer, I. Butterworth, V.L. Harris, G. Howell, B.H.Y. Hung,
L. Lamberti[22], K.R. Long, D.B. Miller, N. Pavel, A. Prinias[23], J.K. Sedgbeer, D. Sideris,
A.F. Whitfield

Imperial College London, High Energy Nuclear Physics Group, London, UK[50]

U. Mallik, M.Z. Wang, S.M. Wang, J.T. Wu

University of Iowa Physics and Astronomy Dept., Iowa City, USA[51]

P. Cloth, D. Filges

Forschungszentrum Jülich, Institut für Kernphysik, Jülich, Germany

S.H. An, G.H. Cho, B.J. Ko, S.B. Lee, S.W. Nam, H.S. Park, S.K. Park

Korea University, Seoul, South Korea [43]

S. Kartik, H.-J. Kim, R.R. McNeil, W. Metcalf, V.K. Nadendla

Louisiana State University, Dept. of Physics and Astronomy, Baton Rouge, LA, USA [51]

F. Barreiro, J.P. Fernandez, R. Graciani, J.M. Hernández, L. Hervás, L. Labarga, M. Martinez, J. del Peso, J. Puga, J. Terron, J.F. de Trocóniz

Univer. Autónoma Madrid, Depto de Física Teórica, Madrid, Spain [49]

F. Corriveau, D.S. Hanna, J. Hartmann, L.W. Hung, J.N. Lim, C.G. Matthews [24], P.M. Patel, M. Riveline, D.G. Stairs, M. St-Laurent, R. Ullmann, G. Zacek [24]

McGill University, Dept. of Physics, Montréal, Québec, Canada [36,37]

T. Tsurugai

Meiji Gakuin University, Faculty of General Education, Yokohama, Japan

V. Bashkirov, B.A. Dolgoshein, A. Stifutkin

Moscow Engineering Physics Institute, Moscow, Russia [47]

G.L. Bashindzhagyan [25], P.F. Ermolov, L.K. Gladilin, Yu.A. Golubkov, V.D. Kobrin, I.A. Korzhavina, V.A. Kuzmin, O.Yu. Lukina, A.S. Proskuryakov, A.A. Savin, L.M. Shcheglova, A.N. Solomin, N.P. Zotov

Moscow State University, Institute of Nuclear Physics, Moscow, Russia [48]

M. Botje, F. Chlebana, J. Engelen, M. de Kamps, P. Kooijman, A. Kruse, A. van Sighem, H. Tiecke, W. Verkerke, J. Vossebeld, M. Vreeswijk, L. Wiggers, E. de Wolf, R. van Woudenberg [26]

NIKHEF and University of Amsterdam, Netherlands [44]

D. Acosta, B. Bylsma, L.S. Durkin, J. Gilmore, C. Li, T.Y. Ling, P. Nylander, I.H. Park, T.A. Romanowski [27]

Ohio State University, Physics Department, Columbus, Ohio, USA [51]

D.S. Bailey, R.J. Cashmore [28], A.M. Cooper-Sarkar, R.C.E. Devenish, N. Harnew, M. Lancaster [29], L. Lindemann, J.D. McFall, C. Nath, V.A. Noyes [23], A. Quadt, J.R. Tickner, H. Uijterwaal, R. Walczak, D.S. Waters, F.F. Wilson, T. Yip

Department of Physics, University of Oxford, Oxford, UK [50]

A. Bertolin, R. Brugnera, R. Carlin, F. Dal Corso, M. De Giorgi, U. Dosselli, S. Limentani, M. Morandin, M. Posocco, L. Stanco, R. Stroili, C. Voci, F. Zuin

Dipartimento di Fisica dell' Universita and INFN, Padova, Italy [41]

J. Bulmahn, R.G. Feild [30], B.Y. Oh, J.J. Whitmore

Pennsylvania State University, Dept. of Physics, University Park, PA, USA[52]

G. D'Agostini, G. Marini, A. Nigro, E. Tassi

Dipartimento di Fisica, Univ. 'La Sapienza' and INFN, Rome, Italy[41]

J.C. Hart, N.A. McCubbin, T.P. Shah

Rutherford Appleton Laboratory, Chilton, Didcot, Oxon, UK[50]

E. Barberis, T. Dubbs, C. Heusch, M. Van Hook, W. Lockman, J.T. Rahn, H.F.-W. Sadrozinski, A. Seiden, D.C. Williams

University of California, Santa Cruz, CA, USA[51]

J. Biltzinger, R.J. Seifert, O. Schwarzer, A.H. Walenta, G. Zech

Fachbereich Physik der Universität-Gesamthochschule Siegen, Germany[38]

H. Abramowicz, G. Briskin, S. Dagan[31], A. Levy[25]

School of Physics, Tel-Aviv University, Tel Aviv, Israel[40]

J.I. Fleck[32], M. Inuzuka, T. Ishii, M. Kuze, S. Mine, M. Nakao, I. Suzuki, K. Tokushuku, K. Umemori, S. Yamada, Y. Yamazaki

Institute for Nuclear Study, University of Tokyo, Tokyo, Japan[42]

M. Chiba, R. Hamatsu, T. Hirose, K. Homma, S. Kitamura[33], T. Matsushita, K. Yamauchi

Tokyo Metropolitan University, Dept. of Physics, Tokyo, Japan[42]

R. Cirio, M. Costa, M.I. Ferrero, S. Maselli, C. Peroni, R. Sacchi, A. Solano, A. Staiano

Universita di Torino, Dipartimento di Fisica Sperimentale and INFN, Torino, Italy[41]

M. Dardo

II Faculty of Sciences, Torino University and INFN - Alessandria, Italy[41]

D.C. Bailey, F. Benard, M. Brkic, C.-P. Fagerstroem, G.F. Hartner, K.K. Joo, G.M. Levman, J.F. Martin, R.S. Orr, S. Polenz, C.R. Sampson, D. Simmons, R.J. Teuscher

University of Toronto, Dept. of Physics, Toronto, Ont., Canada[36]

J.M. Butterworth, C.D. Catterall, T.W. Jones, P.B. Kaziewicz, J.B. Lane, R.L. Saunders, J. Shulman, M.R. Sutton

University College London, Physics and Astronomy Dept., London, UK[50]

B. Lu, L.W. Mo

Virginia Polytechnic Inst. and State University, Physics Dept., Blacksburg, VA, USA[52]

W. Bogusz, J. Ciborowski, J. Gajewski, G. Grzelak[34], M. Kasprzak, M. Krzyżanowski, K. Muchorowski[35], R.J. Nowak, J.M. Pawlak, T. Tymieniecka, A.K. Wróblewski, J.A. Zakrzewski, A.F. Żarnecki

Warsaw University, Institute of Experimental Physics, Warsaw, Poland[45]

M. Adamus

Institute for Nuclear Studies, Warsaw, Poland [45]

C. Coldewey, Y. Eisenberg [31], D. Hochman, U. Karshon [31], D. Revel [31], D. Zer-Zion

Weizmann Institute, Nuclear Physics Dept., Rehovot, Israel [39]

W.F. Badgett, J. Breitweg, D. Chapin, R. Cross, S. Dasu, C. Foudas, R.J. Loveless, S. Mattingly, D.D. Reeder, S. Silverstein, W.H. Smith, A. Vaiciulis, M. Wodarczyk

University of Wisconsin, Dept. of Physics, Madison, WI, USA [51]

S. Bhadra, M.L. Cardy, W.R. Frisken, M. Khakzad, W.N. Murray, W.B. Schmidke

York University, Dept. of Physics, North York, Ont., Canada [36]

Abstract

Jet photoproduction, where the two highest transverse energy (E_T^{jet}) jets have E_T^{jet} above 6 GeV and a jet-jet invariant mass above 23 GeV, has been studied with the ZEUS detector at the HERA *ep* collider. Resolved and direct photoproduction samples have been separated. The cross section as a function of the angle between the jet-jet axis and the beam direction in the dijet rest frame has been measured for the two samples. The measured angular distributions differ markedly from each other. They agree with the predictions of QCD calculations, where the different angular distributions reflect the different spins of the quark and gluon exchanged in the hard subprocess.

1. Introduction

Jet photoproduction at HERA has been used to investigate various aspects of quantum chromodynamics (QCD) and the structure of the photon and the proton [1–6]. QCD calculations of jet cross sections can be factorized into two parts: the parton distributions in the beam particles and the matrix elements of the partonic hard scattering. The selection of the kinematic region and variables in which dijet cross sections are studied can enhance the sensitivity of the data either to the matrix elements or to the parton distributions.

In a previous analysis [6] dijet cross sections were measured in the regime where the difference between the pseudorapidities [53] of the two jets of highest transverse energy ($E_T^{\rm jet}$) is small ($|\eta^{\rm jet1} - \eta^{\rm jet2}| < 0.5$). This constrained θ^*, the angle between the jet-jet axis and the beam axis in the dijet centre of mass system, to be close to 90°. The cross section as a function of $\bar\eta = (\eta^{\rm jet1} + \eta^{\rm jet2})/2$ was then sensitive to the parton distributions in the photon and proton. In contrast, in the present analysis a cut is made on $\bar\eta$, resulting in
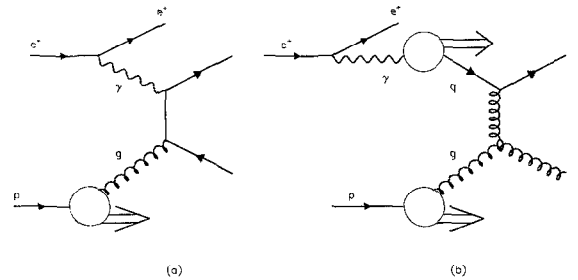

Fig. 1. Examples of LO QCD (a) 'direct' and (b) 'resolved' dijet production diagrams.

a $\cos\theta^*$ distribution which is sensitive to the parton dynamics. The variable $\cos\theta^*$ is calculated as

$$\cos\theta^* = \tanh\left(\frac{\eta^{\rm jet1} - \eta^{\rm jet2}}{2}\right). \tag{1}$$

Only the absolute value of $\cos\theta^*$ can be determined because the outgoing jets are indistinguishable. Measuring the distribution in $\cos\theta^*$ is preferable to measuring the jet pseudorapidity distribution because $\cos\theta^*$ is approximately invariant under the different boosts along the beam axis arising from the spectrum of incoming parton momenta. This minimizes the sensitivity of the cross section to the momentum density distribution of the partons in the beam particles.

In leading order (LO) QCD, two types of processes lead to the photoproduction of jets. In direct processes (Fig. 1a) the photon participates in the hard scatter via either boson-gluon fusion or QCD Compton scattering. These processes involve a quark propagator in the s, t or u channel, with t and u channel processes dominating. In resolved processes (Fig. 1b) the photon acts as a source of quarks and gluons, and only a fraction of its momentum participates in the hard scatter. In this case the dominant subprocesses, e.g. $qg \to qg$, $gg \to gg$ and $qq \to qq$, have t-channel gluon exchange diagrams. The angular dependence of the cross section for resolved processes with a spin-1 gluon propagator is approximately $\propto (1 - |\cos\theta^*|)^{-2}$ (as in Rutherford scattering). This cross section rises more steeply with increasing $|\cos\theta^*|$ than that for direct processes with a spin-$\frac{1}{2}$ quark propagator, where the angular dependence is approximately $\propto (1 - |\cos\theta^*|)^{-1}$. After inclusion of all LO diagrams, QCD predicts that the angular distribution of the outgoing partons in resolved processes will be enhanced at high $|\cos\theta^*|$ with respect to direct photon processes. This property is ex-

pected to be preserved in next-to-leading order (NLO) calculations [7]. In addition to depending upon the incoming flux of partons, this prediction is sensitive to the relative colour factors for each subprocess and to the spins of the quark and the gluon.

The separation between direct and resolved photoproduction is only well defined at LO. To be able to make a measurement which can be compared to calculations at any order, the variable x_γ^{OBS} is used to define these two kinematic regions [6]. The variable x_γ^{OBS} is the fraction of the photon energy contributing to the production of the two highest E_T^{jet} jets. It is defined as

$$x_\gamma^{OBS} = \frac{E_T^{jet1} e^{-\eta^{jet1}} + E_T^{jet2} e^{-\eta^{jet2}}}{2E_\gamma} \qquad (2)$$

where E_γ is the initial photon energy. Direct processes as defined at leading order have high x_γ^{OBS} since all the photon's energy participates in the production of the hard jets, while resolved processes as defined at leading order have low x_γ^{OBS} since part of the photon's energy goes into the photon remnant. Thus the different spins of the quark and gluon propagators that are dominant in the high x_γ^{OBS} and the low x_γ^{OBS} processes respectively should be reflected in the $\cos\theta^*$ distributions of the two samples. Henceforth throughout the following, in both the data and the calculations, direct and resolved samples are defined in terms of a cut on x_γ^{OBS} rather than in terms of the LO diagrams, unless explicitly stated otherwise.

Measurements of dijet angular distributions in $p\bar{p}$ events have shown good agreement with the predictions of perturbative QCD [8] in both fermionic and bosonic exchange processes [9]. The measurement presented here tests QCD in a different kinematic regime and in a different process, and provides an opportunity to study the parton dynamics of two distinct dijet production mechanisms in the same experiment.

2. Experimental setup

In 1994 HERA provided 820 GeV protons and 27.5 GeV positrons colliding in 153 bunches. Additional unpaired positron and proton bunches circulated to allow monitoring of the background from beamgas interactions. Events from empty bunches were used to estimate the background from cosmic rays.

The total integrated luminosity used in this analysis is 2.6 pb^{-1} collected during this running period.

Details of the ZEUS detector have been described elsewhere [10]. The primary components used in this analysis are the central calorimeter and the central tracking detectors. The uranium-scintillator calorimeter [11] covers 99.7% of the total solid angle and is subdivided into three parts, forward (FCAL) covering $4.3 > \eta > 1.1$, barrel (BCAL) covering the central region $1.1 > \eta > -0.75$ and rear (RCAL) covering the backward region $-0.75 > \eta > -3.8$ for an event at the nominal interaction point. Each part consists of an electromagnetic section followed by a hadronic section, with cell sizes of approximately 5×20 cm^2 (10×20 cm^2 in the rear calorimeter) and 20×20 cm^2 respectively. The central tracking system consists of a vertex detector [12] and a central tracking chamber [13] enclosed in a 1.43 T solenoidal magnetic field. A lead-scintillator photon calorimeter is used to measure the luminosity via the positron proton Bremsstrahlung process. This calorimeter is installed 100 m along the HERA tunnel from the interaction point in the positron direction and subtends a small angle at the interaction vertex [14]. Positrons scattered through small angles are detected in a similar lead-scintillator calorimeter.

3. Event selection

The ZEUS detector uses a three level trigger system. At the first level events were triggered on a coincidence of a regional or transverse energy sum in the calorimeter and a track from the interaction point measured in the central tracking chamber. At the second level at least 8 GeV total transverse energy, excluding the eight calorimeter towers immediately surrounding the forward beampipe, was required, and cuts on calorimeter energies and timing were used to suppress events caused by interactions between the proton beam and residual gas in the beam pipe [15]. At the third level, jets were found using the calorimeter cell energies and positions as input to a cone algorithm[16]. Events were required to have at least two jets of $E_T^{jet} > 3.5$ GeV and $\eta^{jet} < 3.0$. Additional tracking cuts were made to reject proton beam-gas interactions and cosmic ray events.

Further cuts are applied offline. Charged current

events are rejected by a cut on the missing transverse momentum measured in the calorimeter. To reject remaining beam-gas and cosmic ray background events, tighter cuts using the final vertex position, other tracking information and timing information are applied. Two additional cuts are made [4], based upon different measurements of the inelasticity, defined in the ZEUS frame as

$$y = 1 - \frac{E'_e}{2E_e}(1 - \cos\theta'_e)$$

where E_e is the energy of the incoming positron and E'_e and θ'_e are the energy and polar angle of the outgoing positron.

(i) Events with a positron candidate in the uranium calorimeter are removed if $y_e < 0.7$, where y_e is the value of y as measured assuming the positron candidate is the scattered positron.

(ii) A cut is made on the Jacquet-Blondel measurement of y [17], $y_{JB} = \sum_i (E_i - E_{zi})/2E_e$, where $E_{zi} = E_i \cos\theta_i$, and E_i is the energy deposited in the calorimeter cell i which has a polar angle θ_i with respect to the measured z-vertex of the event. The sum runs over all calorimeter cells. For any event where the scattered positron entered the uranium calorimeter and either was not identified or gave y_e above 0.7, the value of y_{JB} will be near to one. Proton beam-gas events will have low values of y_{JB}. To further reduce the contamination from both these sources, it is required that $0.15 < y_{JB} < 0.7$. This range corresponds to the true y range of $0.25 < y < 0.8$.

These cuts restrict the range of the photon virtuality to less than ~ 4 GeV^2, with a median of around 10^{-3} GeV^2, which excludes deep inelastic scattering (DIS) events.

To select dijet candidates, a cone algorithm is applied to the calorimeter cells using a cone radius $R = \sqrt{(\delta\phi)^2 + (\delta\eta)^2} = 1$, where $\delta\eta(\delta\phi)$ is the distance in $\eta(\phi)$ of the centre of a calorimeter cell from the jet centre. The jet energy measured in the ZEUS detector has been corrected using the Monte Carlo(MC) events described in the next section. The energy response of the ZEUS calorimeter is estimated by comparing jets found in the hadronic final state of the MC generator to jets found in the simulated detector. The average shift in jet energies is -17% and varies between -10% and -25% depending upon η^{jet}. The de-

scription of the jet energy shift in the MC has been checked using tracking and the incident photon energy deduced from the energy of the electron which is measured in the small-angle electron tagger. This description is accurate to within 5% [5,6]. After this correction, events are required to have at least two jets with $E_T^{jet} \geq 6$ GeV and $\eta^{jet} < 2.5$. For events with three or more jets, the two highest E_T^{jet} jets are used to calculate all jet-related event properties. This procedure is also employed later in all the theoretical and MC predictions shown.

For a given centre-of-mass energy, events at high $|\cos\theta^*|$ have smaller scattering angles and thus lower E_T^{jet}. In order to study the $|\cos\theta^*|$ distribution up to $|\cos\theta^*| = 0.85$ without bias from the E_T^{jet} requirement, a cut of $M_{jj} > 23$ GeV has been applied. M_{jj} is the dijet invariant mass calculated using the relationship

$$M_{jj} = \{2E_T^{jet1}E_T^{jet2}[\cosh(\eta^{jet1} - \eta^{jet2}) - \cos(\phi^{jet1} - \phi^{jet2})]\}^{1/2}, \tag{3}$$

where ϕ^{jet} is the azimuthal angle of the jet in the HERA frame. For two jets back-to-back in ϕ and with equal E_T^{jet}, $M_{jj} \approx 2E_T^{jet}/\sqrt{1 - |\cos\theta^*|^2}$.

Because of the asymmetric beam energies, the two parton centre-of-mass system is typically boosted to the forward direction. For resolved photon processes, this effect is bigger because only a fraction of the photon's momentum participates in the hard scatter. MC simulations show that as a result, a significant fraction of jets are at rapidities ($\eta > 2.5$) where they are not well measured in the ZEUS detector. To remove this bias, a cut $|\bar{\eta}| < 0.5$ was applied, where $\bar{\eta}$, the average η of the two jets, is a measure of the boost of the dijet scattering system in the HERA frame:

$$\bar{\eta} \approx \eta_{boost} = \frac{1}{2}\ln\left(\frac{E_p x_p}{E_\gamma x_\gamma}\right) \tag{4}$$

where x_p and x_γ are the momentum fractions of the incoming partons in the proton and photon respectively and E_p is the incoming proton energy. In a simple (LO) $2 \rightarrow 2$ scatter, the dijet invariant mass is related to x_p and x_γ by

$$M_{jj} = \sqrt{4E_\gamma E_p x_\gamma x_p} = \sqrt{4E_e E_p y x_\gamma x_p}. \tag{5}$$

The requirement that the dijet system has high mass and small boost selects events with γp centre-of-mass

energies mostly above 190 GeV, and suppresses events with low x_γ^{OBS}. Thus the incoming partons have approximately equal and opposite momenta and energies sufficient to produce dijets in a region of good acceptance for a wide range of scattering angles. In the range of x_γ and x_p selected by these cuts the photon and proton parton distributions are fairly well determined by previous measurements [3,5,6,15,18].

After these cuts a total of 4964 events remain with $|\cos\theta^*| < 0.85$, of which 1982 have $x_\gamma^{OBS} < 0.75$ and 2982 have $x_\gamma^{OBS} \geq 0.75$. Events with a third jet which passes the E_T^{jet} and η^{jet} cuts comprise 9% of the final sample. 21% of all events have their scattered positrons detected in the small-angle tagger, as is expected for photoproduction events [5]. The beam-gas background, measured using unpaired bunches, is less than 1%. The contamination from events with photon virtualities greater than 4 GeV^2 is estimated to be 3.3% using simulated deep inelastic scattering (DIS) events.

4. Results and discussion

In Fig. 2 the ZEUS dijet data (black dots) are compared to the results of two QCD MC simulation programs, HERWIG58 [19] (solid lines) and PYTHIA57 [20] (broken lines). The GRV [21] parton distributions are used for the photon and the MRSA [22] parton distributions are used for the proton. The simulation programs are based on LO QCD calculations for the hard scatter and include parton showering and hadronization effects. The minimum transverse momentum of the hard scatter is set to 2.5 GeV. For both programs the direct and resolved photon processes are generated separately and combined according to the ratio of their generated cross sections. The combined MC distributions are then normalized to the number of data events. In the case of HERWIG resolved processes, multiparton interactions are included [23], as this has been shown to improve the simulation of the energy flow around the jet axis in low-M_{jj} events [24]. All the MC events are passed through a detailed simulation of the ZEUS detector and the same jet energy correction procedure as was applied to the data. Fig. 2a shows the distribution of events in E_T^{jet}, which falls steeply with

ZEUS 1994
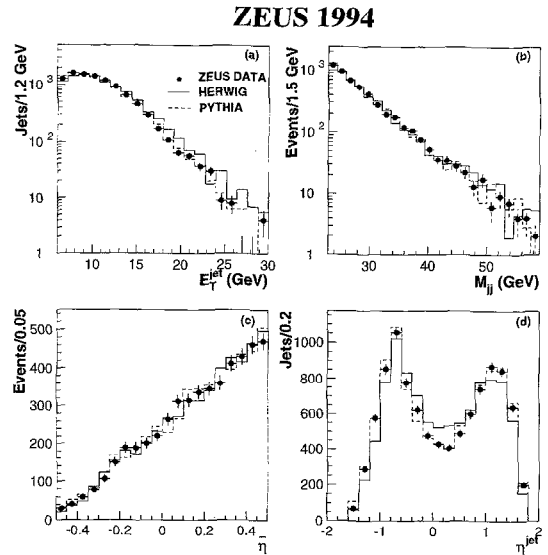
Fig. 2. (a) E_T^{jet}, (b) M_{jj}, (c) $\bar\eta$ and (d) η^{jet} distributions. Raw ZEUS data are compared to the results of the HERWIG58 (solid line) and PYTHIA57 (broken line) Monte Carlo models after simulation of all detector effects and application of selection cuts. The MC samples have been normalized to the number of events in the data. Only statistical errors are shown.

increasing E_T^{jet}. At low E_T^{jet} the dijet mass cut causes the distribution to turn over. Fig. 2b shows the M_{jj} distribution, which falls steeply with increasing M_{jj} and extends to masses of 60 GeV. The $\bar\eta$ distribution is shown in Fig. 2c, and rises with increasing $\bar\eta$ due to the asymmetric momenta of the photon and proton. The $\bar\eta$ cut leads to an η^{jet} distribution which is peaked in the forward and rear directions, as shown in Fig. 2d. Note also that due to the $\bar\eta$ cut, the absolute value of η^{jet} is restricted to be below 1.8. For all these distributions the data are reasonably well described by PYTHIA and HERWIG, although HERWIG gives more jets in the central region in η^{jet} and at high E_T^{jet} than are seen in the data.

Fig. 3a shows the uncorrected x_p^{OBS} distribution, where x_p^{OBS} is the fraction of the proton's energy contributing to the production of the two highest E_T^{jet} jets:

$$x_p^{OBS} = \frac{E_{T1}e^{\eta^{jet1}} + E_{T2}e^{\eta^{jet2}}}{2E_p}. \tag{6}$$

The events lie in the range $0.006 < x_p^{OBS} < 0.06$, with the most probable value at $x_p^{OBS} \approx 0.016$. Fig.

ZEUS 1994

Fig. 3. Raw ZEUS data compared to results of Monte Carlo models after simulation of detector effects and application of selection cuts. (a) x_p^{OBS} and (b) x_γ^{OBS} distr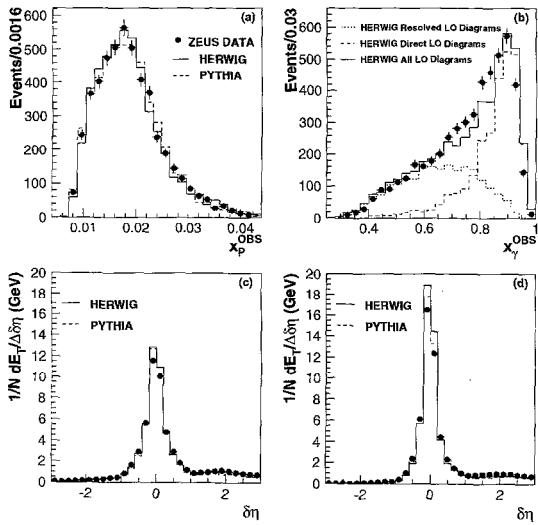ibution. The MC samples have been normalized to the number of events in the data. Figures (c) and (d) show the uncorrected transverse energy flow $1/N dE_T/d\delta\eta$ around the jet axis, for cells within one radian in ϕ of the jet axis, for (c) resolved ($x_\gamma^{OBS} < 0.75$), (d) direct ($x_\gamma^{OBS} > 0.75$) events. Only statistical errors are shown. In (a), (c) and (d), the histograms are HERWIG58 (solid line) and PYTHIA57 (broken line) In (b), the solid line is HERWIG58, the broken line is the distribution of the LO direct diagrams (e.g. Fig. 1a) and the dotted line is that of the LO resolved diagrams (e.g. Fig. 1b).

3b shows the uncorrected x_γ^{OBS} distribution[54]. Contributions from the direct photon LO diagrams (e.g. Fig. 1a) (broken line) and the resolved photon LO diagrams (e.g. Fig. 1b) (dotted line) of HERWIG are shown together with the combined distribution (solid line). PYTHIA events, not shown in the figure, have a similar distribution. The data exhibit a slightly lower mean x_γ^{OBS} than the MC. A cut is applied at $x_\gamma^{OBS} = 0.75$ to define the direct and resolved photon samples. The effect of the imperfect description of the data by MC on the evaluation of the cross sections is evaluated by varying the x_γ^{OBS} cut, and is small. The transverse energy flow around the jets is shown in Fig. 3c for resolved and in Fig. 3d for direct events. In this sample, which has high M_{jj} values, both the HERWIG sample

---

[54] x_γ^{OBS} was measured using the uncorrected jet transverse energies. This takes advantage of cancellations between energy losses in E_T^{jet} and $E_\gamma = y_{JB} E_e$.

with multiple interactions included and the PYTHIA sample without multiple interactions describe the jet profiles reasonably well in both direct and resolved events. The requirements of high mass and small boost remove the disagreement in the forward energy flow between data and the simulations which has been reported elsewhere [3,5,6] in hard photoproduction at HERA.

The resolution of the kinematic variables has been studied by comparing in the MC simulation jets reconstructed from final state particles (hadron jets) with jets reconstructed from the energies measured in the calorimeter (calorimeter jets), and by comparing y_{JB} with the true y. The difference in $|\cos\theta^*|$ between the hadron and detector levels has a mean of zero, a width of 0.03 and is approximately independent of $|\cos\theta^*|$, M_{jj} and $\bar\eta$. The resolution of x_γ^{OBS} is 8.7% at $x_\gamma^{OBS} = 0.75$. For the variables E_T^{jet}, M_{jj} and y, the resolutions are 13.2%, 11.1% and 11.0% respectively at the values at which the cuts are applied.

The MC samples have been used to correct for the efficiency of the trigger and selection cuts and migrations, and for the contamination from DIS events. The final bin-by-bin correction factors are approximately independent of $|\cos\theta^*|$ and are around 1.1 for the resolved and 1.5 for the direct cross section. These correction factors are calculated as the ratio of the purity ($= N_{true,rec}/N_{rec}$) to the efficiency ($= N_{true,rec}/N_{true}$) in each bin. N_{true} is the number of events generated in the bin, N_{rec} is the number of events reconstructed in the bin after detector smearing and all experimental cuts, and $N_{true,rec}$ is the number of events which were both generated in the bin and reconstructed in that bin. The difference between the correction factors for resolved and direct events is due to the fact that the E_T^{jet} and M_{jj} distributions are steeper in resolved processes than in the direct, and thus migrations from below the cuts are more significant, giving a lower purity for resolved than direct.

The sensitivity of the measured cross sections to the selection cuts has been investigated by varying the cuts on the reconstructed variables in the data and HERWIG MC samples and re-evaluating the cross section. In addition, the cross section was re-evaluated using a different ratio of the direct and resolved contributions, and using the PYTHIA sample. The systematic uncertainty arising from the subtraction of the contami-
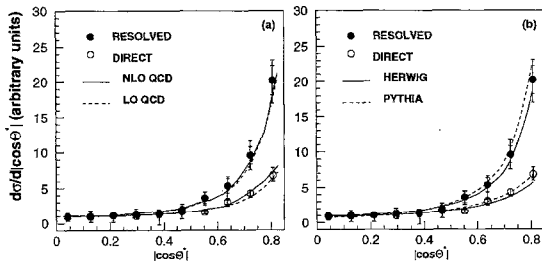
ZEUS 1994

Fig. 4. $d\sigma/d|\cos\theta^*|$ normalized to one at $\cos\theta^* = 0$ for resolved (black dots) and direct (open circles) photoproduction. In (a), the ZEUS data are compared to the NLO prediction (solid line) and the LO prediction (broken line). The parton distribution sets used in the calculation are CTEQ3M [26] for the proton and GRV (LO) [21] for the photon. In (b), the broken line is the PYTHIA distribution and solid line is HERWIG distribution. The inner error bars are the statistical errors, the outer error bars are the sum in quadrature of the statistical and systematic errors, excluding the energy scale and luminosity uncertainties (see Table 1).

nation coming from DIS was estimated by using two different DIS Monte Carlo generators and two different positron-finding algorithms [15,18]. We have also allowed for the possibility that the detector simulation may overestimate the detector energy response by up to 5%, as mentioned in Section 3.

The cross sections $d\sigma/d|\cos\theta^*|$ for $ep \rightarrow$ dijets $+X$ in the range $M_{jj} > 23$ GeV, $E_T^{jet} > 6$ GeV, $|\bar{\eta}| < 0.5$, $0.25 < y < 0.8$ and for virtualities of the exchanged photon < 4 GeV^2 are listed in Table 1. For the direct photoproduction sample the ep cross section rises from around 0.8 nb at $|\cos\theta^*| = 0$ to around 6 nb at $|\cos\theta^*| = 0.85$. For the resolved photoproduction sample the ep cross section rises from around 0.2 nb at $|\cos\theta^*| = 0$ to around 4 nb at $|\cos\theta^*| = 0.85$. In Fig. 4a and b the two cross sections have been normalized to unity at $|\cos\theta^*| = 0$ so that the shapes can be compared directly. To determine the normalization, the 5 lowest $|\cos\theta^*|$ bins were fitted to the functional form expected for the dominant cross section in each sample (as described in Section 1), which is slowly rising in this region. The only free parameter in this fit is the normalisation of the function. The intercept of the function then gives the factor by which the data are divided. In Fig. 4a the data are compared to LO and partial [55] NLO QCD parton level calculations [7]. The

resolved cross section is seen to rise more steeply than the direct cross section with increasing $|\cos\theta^*|$. There is good agreement between data and theory, verifying the expected effects of the spins of the quark and gluon propagators. This is also seen in Fig. 4b, where the data are compared to the HERWIG and PYTHIA predictions. For both of the generators, MRSA(proton) and GRVLO(photon) [21] parton parameterisation sets are used. The MC curves were also made with different parton distribution sets in the photon and proton. The largest change seen was for the LAC1 [25] photon parton distribution set, where there is a 35% increase in the prediction in the highest $|\cos\theta^*|$ bin. In all the calculations, resolved and direct samples are defined on the basis of the cut on x_γ^{OBS}, exactly as in the data. Both the MC and the parton level calculations show the same behaviour, suggesting that the effects of parton showers and hadronisation on this distribution are small. The data are in good agreement with the MC and with the calculations.

The only difference in the cuts applied to the two samples is the cut on x_γ^{OBS} which is used to separate the resolved and direct samples. A MC study has been performed to investigate whether the different behaviour of the two cross sections might be a kinematic effect of this cut. The study shows that the tail of the resolved photon LO diagrams (e.g. Fig. 1b) which lie above $x_\gamma^{OBS} = 0.75$ retain the steeply rising $|\cos\theta^*|$ distribution characteristic of the low-x_γ^{OBS} events. Thus the different behaviour of the two cross sections is due to the different partonic subprocesses which contribute in the different x_γ^{OBS} regions.

5. Summary and conclusion

The dijet angular cross section $d\sigma/d|\cos\theta^*|$, where θ^* is the jet scattering angle in the dijet c.m.s, has been measured for $ep \rightarrow 2$ or more jets with transverse energies $E_T^{jet} \geq 6$ GeV, dijet invariant mass $M_{jj} > 23$ GeV and average pseudorapidity $|\bar{\eta}| < 0.5$, in the range $0.25 < y < 0.8$ and for virtualities of the exchanged photon less than 4 GeV^2. The cross section has been measured for resolved ($x_\gamma^{OBS} < 0.75$) and direct ($x_\gamma^{OBS} \geq 0.75$) processes. The angular dependence for the two samples is significantly different.

---

[55] The NLO calculations do not yet include terms of $O(\alpha_s^3 \times f)$,

where f is the flux of partons in the photon.

Table 1

Differential cross sections $d\sigma/d|\cos\theta^*|$ for $ep \to 2$ or more jets with $E_T^{\text{jet}} \geq 6$ GeV, $M_{jj} > 23$ GeV and $|\bar{\eta}| < 0.5$, in the range $0.25 < y < 0.8$ and for virtualities of the exchanged photon less than 4 GeV^2, for direct and resolved processes. The first column shows the cross section and statistical errors in units of nb, the second column the uncorrelated systematic errors, the third column the shift in the cross section when the correction is evaluated using PYTHIA instead of HERWIG and the fourth and fifth columns the shifts in the cross section when the calorimeter energy calibration is varied by $\pm 5\%$. There is an additional overall uncertainty of 3.3% arising from the luminosity measurement.

$|\cos\theta^*|$ range	Direct (nb / unit $|\cos\theta^*|$)				
	$d\sigma/d|\cos\theta^*| \pm$ stat.	syst. error	PYTHIA	E scale -5%	E scale $+5\%$
0.000 to 0.085	0.80 $\pm$0.12	+0.06/ $-$ 0.09	-0.08	-0.07	0.06
0.085 to 0.170	0.83 $\pm$0.13	+0.07/ $-$ 0.13	-0.10	-0.13	0.11
0.170 to 0.255	0.98 $\pm$0.15	+0.02/ $-$ 0.13	-0.17	-0.16	0.16
0.255 to 0.340	0.90 $\pm$0.14	+0.02/ $-$ 0.08	-0.13	-0.12	0.12
0.340 to 0.425	1.26 $\pm$0.19	+0.15/ $-$ 0.16	-0.30	-0.21	0.26
0.425 to 0.510	1.50 $\pm$0.18	+0.08/ $-$ 0.19	-0.26	-0.26	0.24
0.510 to 0.595	1.41 $\pm$0.17	+0.18/ $-$ 0.08	-0.10	-0.21	0.14
0.595 to 0.680	2.70 $\pm$0.28	+0.36/ $-$ 0.35	-0.27	-0.53	0.51
0.680 to 0.765	3.81 $\pm$0.33	+0.14/ $-$ 0.29	-0.30	-0.57	0.36
0.765 to 0.850	5.99 $\pm$0.48	+0.81/ $-$ 0.40	-0.37	-0.96	0.86

$|\cos\theta^*|$ range	Resolved (nb / unit $|\cos\theta^*|$)				
	$d\sigma/d|\cos\theta^*| \pm$ stat.	syst. error	PYTHIA	E scale -5%	E scale $+5\%$
0.000 to 0.085	0.21 $\pm$0.08	+0.06/ $-$ 0.08	-0.09	-0.04	0.00
0.085 to 0.170	0.23 $\pm$0.12	+0.09/ $-$ 0.12	-0.08	-0.06	-0.02
0.170 to 0.255	0.23 $\pm$0.10	+0.04/ $-$ 0.07	0.01	-0.06	0.12
0.255 to 0.340	0.28 $\pm$0.09	+0.13/ $-$ 0.02	0.00	-0.02	0.04
0.340 to 0.425	0.27 $\pm$0.10	+0.10/ $-$ 0.06	-0.03	0.01	0.02
0.425 to 0.510	0.42 $\pm$0.11	+0.11/ $-$ 0.04	-0.03	-0.06	0.11
0.510 to 0.595	0.77 $\pm$0.17	+0.08/ $-$ 0.08	0.21	-0.13	0.10
0.595 to 0.680	1.13 $\pm$0.21	+0.16/ $-$ 0.26	-0.02	-0.22	0.07
0.680 to 0.765	2.03 $\pm$0.25	+0.36/ $-$ 0.19	0.01	-0.39	0.63
0.765 to 0.850	4.31 $\pm$0.43	+0.47/ $-$ 0.39	0.15	-0.85	0.97

The dependence of $d\sigma/d|\cos\theta^*|$ on $|\cos\theta^*|$ reflects the different spins of the quark and gluon propagators and the relative contributions of the underlying subprocesses in resolved and direct photoproduction. In LO QCD the cross section rises faster with increasing $|\cos\theta^*|$ for resolved photoproduction, where processes involving spin-1 gluon exchange dominate, than for direct photoproduction, where processes involving spin-1/2 quark exchange dominate. These expectations are preserved in NLO QCD calculations and in Monte Carlo simulations which include parton showering and hadronisation models. The $|\cos\theta^*|$ dependence of the measured cross sections is in good agreement with these theoretical predictions and thus confirms fundamental aspects of quantum chromodynamics.

References

[1] H1 Collab., T. Ahmed et al., Phys. Lett. B297 (1992) 205.

[2] ZEUS Collab., M. Derrick et al., Phys. Lett. B297 (1992) 404.

[3] H1 Collab., I. Abt et al., Phys. Lett. B314 (1993) 436.

[4] ZEUS Collab., M. Derrick et al., Phys. Lett. B322 (1994) 287.

[5] ZEUS Collab., M. Derrick et al., Phys. Lett. B342 (1995) 417.

[6] ZEUS Collab., M. Derrick et al., Phys. Lett. B348 (1995) 665.

[7] H. Baer, J. Ohnemus, and J. F. Owens, Phys. Rev. D40 (1989) 2844;
J. F. Owens, private communication.

[8] UA1 Collab., G. Arnison et al., Phys. Lett. B136 (1984) 294;
UA1 Collab., G. Arnison et al., Phys. Lett. B177 (1986) 244;
CDF Collab., F. Abe et al., Phys. Rev. Lett. 62 (1989) 3020.

[9] CDF Collab., F. Abe et al., Phys. Rev. Lett. 73 (1994) 2296.

[10] ZEUS Collab., The ZEUS detector, Status Report (1993).

[11] M. Derrick et al., Nucl. Instr. and Meth. A309 (1991) 77;
A. Andresen et al., Nucl. Instr. and Meth. A309 (1991) 101;
A. Bernstein et al., Nucl. Instr. and Meth. A336 (1993) 23.

[12] C. Alvisi et al., Nucl. Instr. and Meth. A305 (1991) 30.

[13] B. Foster et al., Nucl. Phys. B, Proc. Suppl. B32 (1993) 181.

[14] J. Andruszków et al., DESY 92-066.

[15] ZEUS Collab., M. Derrick et al., Phys. Lett. B316 (1993) 412.

[16] J. Huth et al., Proc. of the 1990 DPF Summer Study on High Energy Physics, Snowmass, Colorado, edited by E.L. Berger (World Scientific, Singapore,1992) p. 134;
UA1 Collab., G. Arnison et al., Phys. Lett. 123B (1983) 115.

[17] F. Jacquet and A. Blondel, in Proceedings of the study of an *ep* facility for Europe, Hamburg, ed. U. Amaldi, (DESY 79/48, 1979) 391.

[18] ZEUS Collab., M. Derrick et al., Zeit. f. Phys. C65 (1995) 379;
H1 Collab., T. Ahmed et al., Nucl. Phys. B439 (1995) 471;
ZEUS Collab., M. Derrick et al., Zeit. f. Phys. C69 (1996) 607.

[19] G. Marchesini et al., Comp. Phys. Comm. 67 (1992) 465.

[20] H.-U. Bengtsson and T. Sjöstrand, Comp. Phys. Comm. 46 (1987) 43;
T. Sjöstrand, CERN-TH.6488/92 (1992).

[21] M. Glück, E. Reya and A. Vogt, Phys. Rev. D46 (1992) 1973.

[22] A. Martin, W.J. Stirling and R.G. Roberts, Phys. Rev. D50 (1994) 6734.

[23] T. Sjöstrand and M. van Zijl, Phys. Rev. D36 (1987) 2019;
G. A. Schüler and T. Sjöstrand, Phys. Lett. B300 (1993) 169; Nucl. Phys. B407 (1993) 539;
J. M. Butterworth and J. R. Forshaw, J. Phys. G19 (1993) 1657;
J. M. Butterworth, J. R. Forshaw and M. H. Seymour, CERN-TH-95-82, to appear in Zeit. f. Phys. C.

[24] H1 Collab., S. Aid et al., Zeit. f. Phys. C70 (1996) 17.

[25] H. Abramowicz, K. Charchula and A. Levy, Phys. Lett. B269 (1991) 458.

[26] CTEQ Collab., J. Botts et al., Phys. Lett. B304 (1993) 15;
CTEQ Collab., J. Botts et al. (to be published).